UNIVERSITY OF CALIFORNIA SAN DIEGO

A Cell-Cycle Dependent Regulation Of A Delayed Negative Feedback In IFN-α Signaling

A Thesis submitted in partial satisfaction of the requirements

for the degree Master of Science

in

Biology

by

Bingxian Xu

Committee in charge:

Professor Nan Hao, Chair
Professor Elena Koslover
Professor Sergey Kryazhimskiy

2020

The Thesis of Bingxian Xu is approved, and it is acceptable in quality and form for publication on microfilm and electronically:

Chair

University of California San Diego

2020

Table of Contents

Acknowledgements

I would like to acknowledge professor Nan Hao for his support as the chair of my committee and for his unfounded trust when he assigned me the project. Never realized my work could actually be published so much later after that, it was a moment to remember. And how amazing it is to get a monitor!

I would like to acknowledge professor Elena Koslover for all the discussions we had, and all the help given to me during my application process. I was told time and time again how criticism should be voiced more constructively during an interview, which in hindsight, I probably should have done that.

I would like to acknowledge Yanfei Jiang for the guidance that was given to me and for always pushing to do things I don't want to do.

I would also like to acknowledge Anusorn Mudla, who was responsible for all the experimental work. Without him, I would not even be able to graduate.

This thesis, in full, is a modified version of an article that is being prepared for submission for publication. Anusorn Mudla, Bingxian Xu, Keiichiro Arimoto, Adarsh Rajesh, Andy Ryan, Wei Wang, Matthew D Daugherty, Yanfei Jiang, Dong-Er Zhang, and Nan Hao. The thesis author was one of the authors of this material.

LIST OF FIGURES

Abstract of the thesis

A Cell-Cycle Dependent Regulation Of A Delayed Negative Feedback In IFN-α Signaling

By

Bingxian Xu

Master of Science in Biology

University of California San Diego, 2020

Professor Nan Hao, chair

Interferon-alpha (IFN-α) is a major cytokine produced in response to viral infection and clinically important in anti-viral and anti-cancer therapy. Although several key components of the interferon pathway have been characterized, their dynamics in response to repetitive stimulation remain elusive. Here, we studied how IFN-α pretreatment can lead to two

contradictory effects: priming and desensitization. We used a microfluidic device to control the dynamics of IFN-α stimulation. Single cell quantification from time-lapse microscopy revealed that 2- and 10-hour pretreatment can lead to increased cellular response while 24-hour pretreatment lead to a decrease cellular response both in STAT1 nuclear translocation and the rate of IRF9 induction. To further investigate the mechanism, we knock-downed ubiquitin specific protease 18 (USP18), a known negative regulator of IFN-α signaling using shRNA, and found that STAT1 nuclear translocation was restored and the rate of IRF9 induction was significantly higher. Intriguingly, we observed heterogeneity in the desensitization among 24-hour-pretreated cells of which expressed low level of USP18. We developed a mathematical model to describe and predict the effect of pulsatile IFN-α stimulation. As expected, a pulsatile treatment of IFN-α led to higher IRF9 induction compared to a sustained treatment. Our results demonstrate that priming and desensitization of IFN-α is duration dependent and controlled by USP18 as a delayed negative feedback. This discovery provides insight information to improve pharmacokinetic of IFN-α delivery for more effective viral-infected disease and cancer therapy.

Introduction

IFN-α is a major Type I cytokine regulating the function of the immune system against viral infection, intracellular pathogen and cancer development. IFN-α exhibits its anti-pathogenic and anti-proliferative effects via expression of over 300 interferon stimulated genes (ISGs), of which enables effective host pathogen defense, modulates immune responses and hinders uncontrolled cell growth[3,10]. IFN-α has been clinically used in treatments of variety diseases such as hepatitis B and C infection, melanoma, kidney cancer, leukemia and lymphoma. However, studies have shown that inappropriate IFN-α activation contributes to pathogenesis of myriad diseases such as rheumatoid arthritis, systemic lupus erythematosus and several forms of interferonopathies. Despite decades the remarkable perspicacity in identifying the key components in the pathway, there are limited number of information about the dynamics of those molecules and how they regulate the outcome of IFN-α treatment. In addition, the lack of refined experimental data in the dynamics of those cellular components limit the development of mathematical model to recapitulate the system.

The binding of IFN-a to the cognate receptors, IFNAR1 and IRNAR2, causes receptor dimerization and conformational changes that triggers the cross-activation of receptor-associated kinases: JAK1 and TYK2, that in-turn phosphorylate the intracellular tail of the receptors allowing the docking of STAT1 and STAT2. The tyrosine kinases phosphorylate STAT1 and STAT2 heterodimerize and bind to IRF9 to form interferon stimulated gene factor 3 (ISGF3) complex. ISGF3 translocates to the nucleus and binds to interferon-stimulated response element (ISRE) sites on the promoter or enhancer region of the responsive genes[4]. Several of these genes acts as positive feedback while others are negative feedback.

Cells previously exposed to IFN-α showed two distinct phenotypes: priming and desensitization. Priming defines as the increase in cellular responses to the second stimulation while desensitization is the opposite. IFN-α priming accelerates the production of IFN and enhanced the translation of IFN mRNA[1] and can also completely change the cellular responsiveness viral infection[2] such as SARS coronavirus[3] and influenza virus[4]. The mechanisms of priming have been proposed involving the production of STAT1, STAT2 and IRF-9[5]. However, there are more work to be done to fully understand the dynamics of these positive feedback molecules. On the other hand, IFN-α treatment causes long-lasting refractoriness[7] and inactivates the IFN-α responses[6]. The mechanism of desensitization involved the induction of negative feedback molecules such as SOCS1, SOCS3, SHP2, PIAS, and USP18.

Here we report the time-dependent mechanism of differential response to IFN-α treatment. Using time-lapse imaging and single cells analysis, we showed that cells decouple the priming and desensitization via fast positive feedback and delayed negative feedback respectively. We illustrated that USP18 is the key negative feedback molecule responsible for desensitization and dampen the priming effect. We also developed a mathematical model to predict how pulsatile treatment of IFN-α could boost the effectiveness of IFN-α treatment, in other words, we have identified a way to utilize the innate circuit of the cell to enable a frequency response. By looking deeper into the circuit though more experiments and simulation, we have confirmed that the cells' ability to understand frequency comes from the nature of the delayed negative feedback, USP18. We found that USP18 delay is highly correlated with the cell cycle phase and this coupling is quintessential for our observed frequency response. This study not only provides more complete understanding of IFN-α signaling but also offer an explanation for the frequency response that had been observed in other biological systems[11,12,13,14,15,16]. By having components inside a signaling

pathway coupled with the cell cycle which is itself periodic, the output of the said pathway would then be able to respond to the frequency of the input.

Methods

Cell cultures, transfection and treatment

HeLa and HEK293T cells were cultured in Dullbecco minimal essential medium (DMEM: Thermo Scientific HyClone #SH30022FS) supplemented with 10% fetal bovine serum, 4mM L-glutamine, 100 I.U./mL penicillin and 100 ug/mL streptomycin at 37C, 5% CO2 and 90% humidity. The imaging media is phenol red free DMEM (Life Technology-Gibco) with identical supplements as the cultured medium. The transfections were performed with 1 ug DNA: 2 uL Fugene HD (Promega E2311) ratio. Cells were seeded at 300,000 cells/well in 6-well plate for 18 hours before transfection. Two days after transfection puromycin was added to the medium at 1 ug/mL, and cells were selected for 2 days. Survival cells were grown for another 7 days before sorted with FACS into 96-well and expanded into monoclonal cell lines.

Drug treatments

Cells were treated with 100 ng/mL recombinant human IFN-alpha (Prospec). Lovastatin (Selleck Chemicals, S2061) was used at 5 micromolar and Roscovitine (Sigma-Aldrich, R7772) was used at 5 micromolar as pretreatment for 36 hours prior to IFN-alpha treatment. Decitabine (Sigma-Aldrich, A3656) was used at 100 micromolar for 48 hours prior to IFN-alpha treatment.

Cell line construction

We followed the CRISPR/Cas9 protocol to construct the reporter cell line. In general, the gRNAs were designed by online CRISPR tool (http://crispr.mit.edu) and the DNA oligos were ordered from Eurofins Genomics, annealed and cloned into pSpCas9(BB)-2A-GFP (Addgene #48138) or pSpCas9(BB)-2A-Puro (Addgene #48139) vector plasmids. Plasmids were transfected into HEK293T cells and tested for gRNA efficiency using the T7 endonuclease assay. The donor

plasmids were constructed using Gibson assembly method. We used site-directed in-vitro mutagenesis to make mutations in the donor plasmids to avoid gRNA recognition and Cas9 cutting of the linearized donor.

The donor DNA of nuclear marker has two synonymous mutations (C(30,33) >T mutations) to remove gRNA recognition sequence. The mutations remove SalI site which allow for checking of the correct insertion in the genomic DNA. The STAT1 donor has a C>G mutation in the 3'UTR to remove the PAM the gRNA recognition sequence. Finally, the donor for the IRF9 also has a C>G mutation to remove the PAM sequence.

In more detail, we first developed a nuclear marker cell line by nuclear localization signal inserting nuclear localization signal followed by two copies of infrared fluorescent protein (NLS-2*iRFP) under the endogenous actin promoter with a P2A spacer in HeLa cells. This cell line ensures a constitutive expression without introducing exogeneous strong constitutive promoter and greatly assists cell tracking. We sorted single cell into 96-well plate to obtain homogeneous clones. A minimal of 10 clones are genotyped and checked for homozygosity and correct integration using at least 3 pairs of primers and confirmed with sequencing. A positive clone is further validated with western blot to ensure correct protein expression. To check for the off-target editing, CRISPR Off-target Sites with Mismatches, Insertions, and Deletions (COSMID) is used to search the genomes for potential off-target sites based on guide strand and other parameters (PMID: 25462530). At least 5 top-ranked potential off-target sites are checked by PCR and sequencing. Clones with off-target modifications are discarded. After construction and validation, the engineered single-clonal cell line is assigned a unique identification number, entered in our electronic database, and stored in liquid nitrogen with a cryoprotectant. The same procedure was performed for CRISPR-based tagging the additional genes, STAT1, IRF9 and USP18 sequentially.

The knockdown of USP18 by shRNA using retrovirus transduction in pSuper-Retro-Puro vector from OligoengineTM. The sequence of the shRNA is: taaaaaaggagaagcattgttttcaaa tctcttgaatttgaaaacaatgcttctcctggg. The negative control sequence is: taaaaacagtcgcgtttgcgactggtctcttgaaccagtcgcaaacgcgactgggg.We screened with puromycin and confirmed the presence of the construct in the cells with PCR and confirmed the knock-down of USP18 with western blotting.

For the cell cycle reporter cell lines, we transfected USP18 CRISPR constructs into the nuclear marker cell line and screened for a correct and homogenous monoclonal clone. We then used lentivirus to stably integrate pCMV-DHB-mCherry or pCMV-mCherry-Geminin(1-110)-P2A-mCitrine-Cdt1(30-120) in pLenti-Puro (Addgene: 39481).

Microfluidics and time-lapse imaging

HeLa cells were washed with dPBS and detached from the culture dish with 0.25% trypsin EDTA, centrifuged at 200 rcf for 3 min and resuspended with the complete imaging media at a density of 7-10 million cells per mL. The suspension was loaded into the microfluidic device and allow the cells to adhere for at least 36 hours in the standard incubator. The device was set up with the microscope Nikon Ti under 5% CO2 and 37C. The flow of the media was 1 mL/hour and the control of the valves were done with customized Arduino board. The images were acquired every 5 minutes for phase, Cy5 and mCherry channel and every 20 min for YFP using NES element software. The images were analyzed with customized MATLAB.

Image acquisition

The images were acquired using a Nikon Ti-E inverted microscope equipped with integrated Perfect-Focus (PFS), Nikon Plan Apochromat Lambda 10x objective lens, Nikon Apochromat 20x and Evolve 512 EMCCD camera (Teledyne Photometrics). Time-lapse imaging was performed with an on-stage incubator equipped with temperature control and humidified 5% CO2. Images were taken every 5 minutes for phase, Cy5 and mCherry channel and every 20 min for YFP and 30 min for CFP using Nikon NES element software.

Image analysis and cell tracking

Illumination correction was performed using ImageJ "rolling ball" background subtraction algorithm with 50-pixel radius. Single-cell segmentation, tracking and quantification were performed using a custom MATLAB code developed in our lab. Nuclei were segmented using NLS-2*iRFP intensity and then refined by marker-based watershed and the mask was generated. The phase images were used to generate masks for cell segmentation. The masks were applied to other channels to quantify fluorescent intensity.

Model

The simplified kinetic model of the JAK-STAT signaling pathway consists of two species, USP18 and IRF9, and they negatively and positively regulating the expression of both proteins respectively. The positive feedback from IRF9 is represented by the function,

$$pf = k_1 \cdot \frac{IRF9}{k_2 + IRF9}$$

and the negative feedback from USP18 is represented by the function,

$$nf = \frac{k_3}{k_3 + USP18}$$

The entire network of USP18 and IRF9 is represented by the system of differential equations

$$\frac{d}{dt} IRF9 = I(t) \cdot (k_4 + pf) \cdot nf$$

$$\frac{d}{dt} USP18 = I(t) \cdot S_u (k_5 + pf) \cdot nf - k_6 \cdot USP18$$

S_u directly depends on the dynamics of IFN-α(I) stimulation:

$$S_u = \begin{cases} = 1, if\ d(I) \geq \tau \\ = 0, if d(I) < \tau \end{cases}$$

where d(I) is the duration of IFN-α stimulation at the given time.

ODE solver

The ordinary differential equation (ODE) based model was solved using custom MATLAB code based on Euler's method.

Fitting

Fitting was done using MATLAB built in function, lsqcurvefit. The dynamics of IRF9 under prolonged IFN-α stimulation and the experimental result from the priming experiment were used to fit the model.

The best parameters obtained are summarized in the table:

τ	Cell cycle induced delay (hr)	8
k_1	Positive feedback strength (hr^{-1})	30.6
k_2	Positive feedback saturation constant	297.8
k_3	Negative feedback saturation constant	550.0
k_4	IRF9 production rate (hr^{-1})	2.66
k_5	USP18 production rate (hr^{-1})	66.6

k_6	USP18 degradation rate (hr^{-1})	0
$IRF9_0$	IRF9 initial condition (a.u.)	45
$USP18_0$	USP18 initial condition (a.u.)	0

Cell cycle transcriptionally activity estimation

With knowledge of the cell-cycle induced delay, we further assumed that the activation time, T, that we quantified can be broken down into two parts, such that $T = \tau + T_c$, where τ is the cell cycle independent response time of the pathway and T_c is the delay induced by the cell cycle, both of which a random variable. The probability distribution function of, T, the sum of the two would then be the convolution of their individual probability densities, namely:

$$P(T = t) = \int_0^t P_\tau(\tau') \cdot P_{T_c}(t - \tau')d\tau'$$

From our simulation of cell cycle dependent delay, we have found the distribution of T_c to be:

$$P_{T_c}(T_c = t) = \begin{cases} \dfrac{t_a}{t_{tot}}, & t = 0 \\ \dfrac{1 - \dfrac{t_a}{t_{tot}}}{t_{tot} - t_a}, & 0 \le t \le t_{tot} - t_a \end{cases}$$

Where t_a is the duration of time within a cell cycle where transcription is allowed and t_{tot} is the length of the cell cycle.

By assuming the probability distribution for the cell cycle independent response time to be a gaussian:

$$P_\tau(\tau = t) = \frac{1}{\sigma\sqrt{2 \cdot \pi}} e^{-\frac{1}{2}\left(\frac{t-\mu}{\sigma}\right)^2}$$

The convolution of these two distributions can be computed numerically and its results were fitted to the CFP activation time. The fitted result suggested that the cell cycle has a length of 21.7 hours and the transcriptionally active window of 9.3 hours.

Stochastic simulation

With knowledge of the cell cycle has a length of ~22 hours and an active window of ~9 hours, we first computed a single cell cycle profile, a function that represents the transcriptional activity of USP18 promoter as a function of the cell cycle phase:

$$C(p) = \begin{cases} 1, & p \leq 9 \\ 0, & p > 9 \end{cases}, 0 \leq p \leq 22$$

A cell would start at a randomly phase, p, of the cell cycle, the activation time of USP18 would be the time it takes for the cell to reach a phase of the cell cycle where its transcription activity becomes 1.

Stochastic simulation was then ran with the following stochastic differential equations, whose activation time is set by the starting phase of the cell cycle.

$$\frac{d}{dt} IRF9 = I(t) \cdot (k_6 + pf) \cdot nf + \xi_{IRF9}$$

$$\frac{d}{dt} USP18 = I(t) \cdot S_u (k_8 + pf) \cdot nf - k_9 \cdot USP18 + \xi_{USP18}$$

$$S_u = \begin{cases} = 1, if\ d(I) \geq \tau(p) \\ = 0, if d(I) < \tau(p) \end{cases}$$

Activation time quantification

The activation time of IRF9 and USP18 expression is quantified using costumed MATLAB code. The code breaks the expression dynamics of the gene into two parts, with the first capturing the unchanging gene expression before activation, and the second capturing the increasing gene expression under IFN-α stimulation. By fitting the first part with a zero-order polynomial and the second with a first-order polynomial, scanning across all possible time points, the activation time of gene expression is the time point that gives the lowest error. To further reduce error in the quantification method, only parts of the expression dynamics is used to quantify the activation time. By first fitting the smooth gene expression with the function,

$$X = k_1 + \tanh\big(k_4 \cdot (time - k_2)\big) \cdot k_3$$

the maximum time point scanned is set by k_2, which corresponds to the time when the gene stops increasing linearly. Note, the parameters here are a different group of parameters used for the kinetic model.

Results

Single Cell Response Under IFN-alpha Treatment

In order to monitor the activity of the JAK-STAT signaling pathway at a single cell level, we constructed a reporter cell line in Hela Cells, in which STAT1 was C-terminally tagged with mCherry at its native locus using CRISPR/Cas9 To monitor its downstream response, YFP was inserted under the endogenous promoter of a representative ISG, IRF9 (fig. 1A). Using this cell line and time-lapse microscopy, we can simultaneously track the activity of STAT1 and IRF9 on the single cell level as well as statistics through time (fig. 1B, 1C).

To examine our cell line's response to dynamical IFN-alpha stimulation, we exposed the cells to pulses of IFN-alpha treatment with different durations, followed by an 8-hour break. After that, we applied another 10hr long IFN-alpha treatment (fig. 1D,1E).

Mechanism of Priming and Desensitization

By applying two pulses of IFN-alpha stimulation, using the first as a pretreatment for the cells, we have observed that IRF9 induction level depends on the duration of the pretreatment time in a nonlinear fashion. When the cells were pretreated for 2 or 10 hours, IRF9 induction increases upon the second stimulation compared to control, which we called it priming. However, when the cells were pretreated for 24 hours, IRF9 induction drops (fig. 1F), which we called desensitization.

We next sought to understand the mechanism for the observed nonlinearity. Previous studies have shown that priming effect can be attributed to the expression of IRF9 and STAT1, which are components of the ISGF3 transcriptional complex that regulates cellular response toward IFN-alpha[8]. To identify the mechanism for desensitization, we conduced knock-down

experiment of ubiquitin-specific peptidase 18 (USP18), one of the negative regulators of the JAK-STAT signaling pathway. USP18 inhibits signal transduction on the receptor level and USP18KO cell lines showed no sign of desensitization, all IRF9 induction were similarly increased across all 3 pretreatment times (fig. 2).

Based on these results, we hypothesized that short IFN-alpha treatment activates IRF9 and STAT1, genes that act as positive regulators, whereas long IFN-alpha treatment will lead to the activation of negative regulators of the pathway such as USP18. This separation of time scale between the positive and negative regulator is the key to the nonlinear behavior of the JAK-STAT signaling pathway under dynamical IFN-alpha stimulation.

Computational Modeling Suggests a Delayed Negative Feedback Loop Through USP18

From our experimental results, we postulated that the opposite effects induced by short versus prolonged pretreatment inputs might be caused by different expression kinetics of ISGF3 components and USP18: a short input is sufficient to trigger ISF3 expression and thereby the priming effect, whereas a prolonged input is required to induce USP18 expression and hence desensitization. To test this hypothesis in silico, we devised a simple mathematical model, which is composed of two ordinary differential equations that govern the expression of IRF9, an ISGF3 component, and USP18, respectively. In this model, IRF9 and USP18 act as a positive and negative feedback, respectively, to the expression of both IRF0 and USP18. The only difference between USP18 and IRF9 expression is that of USP18 requires a continuous stimulation that last longer than a threshold (fig. 3A). This model was able to capture the results of the priming experiment (fig. 3C), where priming effect dominates for short pretreatment and desensitization effect dominates when pretreatment time increases. By fixing the threshold for activation, a minimum min error between simulation and experimental result was consistently observed when

the expression of USP18 requires a prolonged stimulation of 8 hours (fig. 3B). This observation is in line with our hypothesis that a continuous input is required to induce USP18, therefore when stimulation time is short, ISGF3 expression dominates the regulation of JAK-STAT pathway, and as stimulation time increases, USP18 starts to take the dominant role.

Furthermore, the model predicts that if sequential pulses of IFN-alpha with duration less than 8hr is given, USP18 will not be activated and the priming effect is dominant. Whereas if a single long pulse is given, with area under the curve being the same as short sequential pulses, USP18 will be activated leading to a lower IRF9 expression (fig. 3D). This hypothesis is tested experimentally and a higher IRF9 expression is observed, congruent with the hypothesis, when 5 8-hr pulse of IFN-alpha stimulation is given compared to a single 40hr pulse. Furthermore, we probed the effect of the removal of the negative feedback. The model predicted that when negative feedback was removed, IRF9 induction would be the same with inputs that share the same area under the curve, which was also observed experimentally in our USP18KO cell line (fig. 3F).

USP18 expression displays cell cycle dependence

To understand the mechanism delayed USP18 activation, we quantified the activation time of both USP18 and IRF9 under prolonged IFN-alpha treatment. Interestingly, we noted that the spread of activation times of USP18 differs significantly from that of IRF9 (fig. 5). Since all the cells used in our experiment are genetically identical, we hypothesized that the difference we observed was under the influence of the cell cycle. To test whether USP18 expression periodicity shows cell cycle dependence, we inferred cell cycle phases of approximately 1500 cells. Our results showed that USP18 activation time is clearly dependent on cell cycle phase (fig. 4, left most panel). When we further color-coded the cells based on whether the cells were activated in

the same cell cycle the stimulus was given, our data formed two very distinctive clusters (fig. 4, mid panel). Based on the linear correlation observed between activation time and cell cycle phase in each cluster, we hypothesized that USP18 expression is only allowed during a certain phase of the cell cycle. From the data, we successfully inferred that this transcriptional active window started at the 5^{th} hour of the cell cycle and lasted for 9 hours (fig. 4, right panel). To further confirm our hypothesis, we constructed the distribution of the activation time, and inferred the cell cycle length and the width of the window from the distribution that we measured (fig. 6, method used is outlined in METHODS). Our inferred result suggested that the cell cycle length is 21.95 hours, and the window width is 9.15 hours.

The data and our data driven inference pointed to the conclusion that at least part of USP18 activation is due to the cell cycle. When IFN-alpha stimulation hits during the off-phase of the cell cycle, USP18 expression will only be allowed after the cell cycle reaches the on-phase, thus creating the observed delay in activation time.

Discussion

The ability to ward off infection is the most essential need for a cell and interferon pathway is one of the major pathways involved viral infection response. As observed, cells pre-exposed to IFN-alpha treatment react to future IFN-alpha treatment more strongly, a phenomenon termed priming[2,3]. On the other hand, pre-exposed cells could also show a weaker response toward future treatment, a phenomenon called desensitization. Both of these affects are vital for cell survival and therefore it is essential to tune the extent of priming and desensitization based on environmental cues. Overreaction due to priming and lead to excessive tissue damage and cytokine storm[9,10]. On the other hand, irresponsiveness due to desensitization will render the cells unprotected during viral infection. Because of this, it is the most important thing to understand how cells responds to dynamical IFN-alpha treatment in order to provide better care to patients with the use of interferon in therapies.

Before our work, the mechanism of priming and desensitization remains largely unknown. In addition, the limited existing literature focuses on population response, ignoring all heterogeneity. Our ability to track single cell expression dynamics of IRF9 and USP18 revealed the underlying mechanism of how the JAK-STAT pathway is regulated, namely, the coupling of a fast positive feedback and a slow negative feedback. We observed that short IFN-alpha treatment lead to the activation of the fast positive feedback thus priming. However, when treatment time lengthens, USP18 becomes activated, leading to desensitization effect. This idea was substantiated by the mathematical model and the model successfully predicted the behavior of the system under short sequences of IFN-alpha treatment compared to a prolonged treatment with the same area under the curve. Suggesting again that the activation of USP18 requires longer IFN-alpha treatment.

Moreover, with the ability to look at USP18 expression dynamics on the single cell level, we were able to observe the mild correlation between USP18 expression and the cell cycle, one invisible on a population scale. This observation drove us to look deeper into the relationship between USP18 activation time and cell cycle phase and led to the discovery of a method that allowed us to accurately infer at the phases of the cell cycle when USP18 expression is allowed.

The idea of having to wait for certain phases of the cell cycle is congruent with the model setup for USP18 expression. For short duration stimulation, it is less likely that the IFN-alpha treatment hit the on-phase of the cell cycle, therefore USP18 is less likely to be activated. When treatment time lengths, it becomes more and more probable to hit the on phase, increasing the chance of USP18 expression. This coupling between a negative regulator and the cell cycle provided a basis for the cell to read dynamical input, or in other words, frequency. As shown both by model and experiment, short pulses of IFN-alpha activate less USP18, and lead to increased IRF9 induction, whereas prolonged IFN-alpha treatment with the same area under the curve would induce USP18 and lowered IRF9 induction. The mechanism that we have discovered can be a widespread mechanism for frequency response for its simplicity. Moreover, the cell cycle dependence of USP18 activation suggests that the treatment of cancer can be further specified by the tumors' preferred cell cycle phase.

Acknowledgements:

This thesis, in full, is a modified version of an article that is being prepared for submission for publication. Anusorn Mudla, Bingxian Xu, Keiichiro Arimoto, Adarsh Rajesh, Andy Ryan, Wei Wang, Matthew D Daugherty, Yanfei Jiang, Dong-Er Zhang, and Nan Hao. The thesis author was one of the authors of this material.

Figures

Figure 1: IFN-alpha pretreatments confer opposite effects depending on their durations

(A) (top) Schematic of HeLa cell line reporter engineered using CRISPR/Cas9. STAT1 was tagged with mCherry at C-terminus to monitor the translocation and its expression. The coding sequence for P2A-YFP was inserted at the C-terminus of IRF9 coding sequence to generate a transcription reporter (PIRF9). (bottom) A simplified IFN-alpha pathway monitored in the study. IFN-alpha treatment leads to STAT1 phosphorylation, ISGF3 complex formation, nuclear translocation and activation of the downstream transcription reporters.

(B) Time lapse images of a representative cell showing fluorescent signal after treated with 100 ng/ml IFN-alpha for 48 hours. The outline represents the nucleus and cell boundaries. Scale bar: 20 μm. The dynamic of different fluorescent signal quantification is shown on the right. The dash lines represent cell divisions.

(C) The averaged fluorescent signal from single cells (n = 257 cells). Data are represented as mean (solid lines) and $\pm$ SD (shaded area). Left: the ratio between nuclear STAT1 and cytoplasmic STAT1. Middle: IRF9 transcription was inferred from YFP expression (PIRF9). Right: IRF9 promoter activity calculated from the derivative of PIRF9 expression in single cells.

(D) Top: The diagram of repetitive IFN-alpha experiment. Cells were pretreated with 100 ng/ml IFN-alpha for 0, 2, 10 and 24 hours followed by 8 hours of "break time" and re-stimulated with IFN-alpha for an additional 10 hours. Bottom: The illustration of the microfluidic set-up. Two syringes filled with culture medium with or without IFN-alpha were connected to a programmable Arduino controlled valves of which manage the duration of IFN-alpha treatment. Images were captured with 10X objective every 5 min throughout the total 52-hour experiment.

(E) Left: the averaged PIRF9-driven gene expression after the second IFN-alpha treatment. The averages were calculated from 3 independent experiments. The blue shading represents the presence of the 10-hour of the second 100 ng/ml IFN-alpha treatment. The level of PIRF9 was normalized to the same level when IFN-alpha was added to make it easier to compare the rate of induction in each pre-treatment condition. Right: IRF9 promoter activity calculated from the derivative of PIRF9-YFP induction. The promoter activity represents the transcription rate of IRF9 promoter.

(F) Left: the bar graph of the average PIRF9 induction upon second IFN-alpha treatment from three independent experiments. Data are represented as mean $\pm$ SEM. The 24-hr pretreatment shows significant decrease in PIRF9 induction. Right: the violin plot of PIRF9 induction upon second stimulation in single cells. The PIRF9 induction was calculated as the additional increase in YFP signal only to the second IFN-alpha treatment. The cells were combined from the 3 experiments.

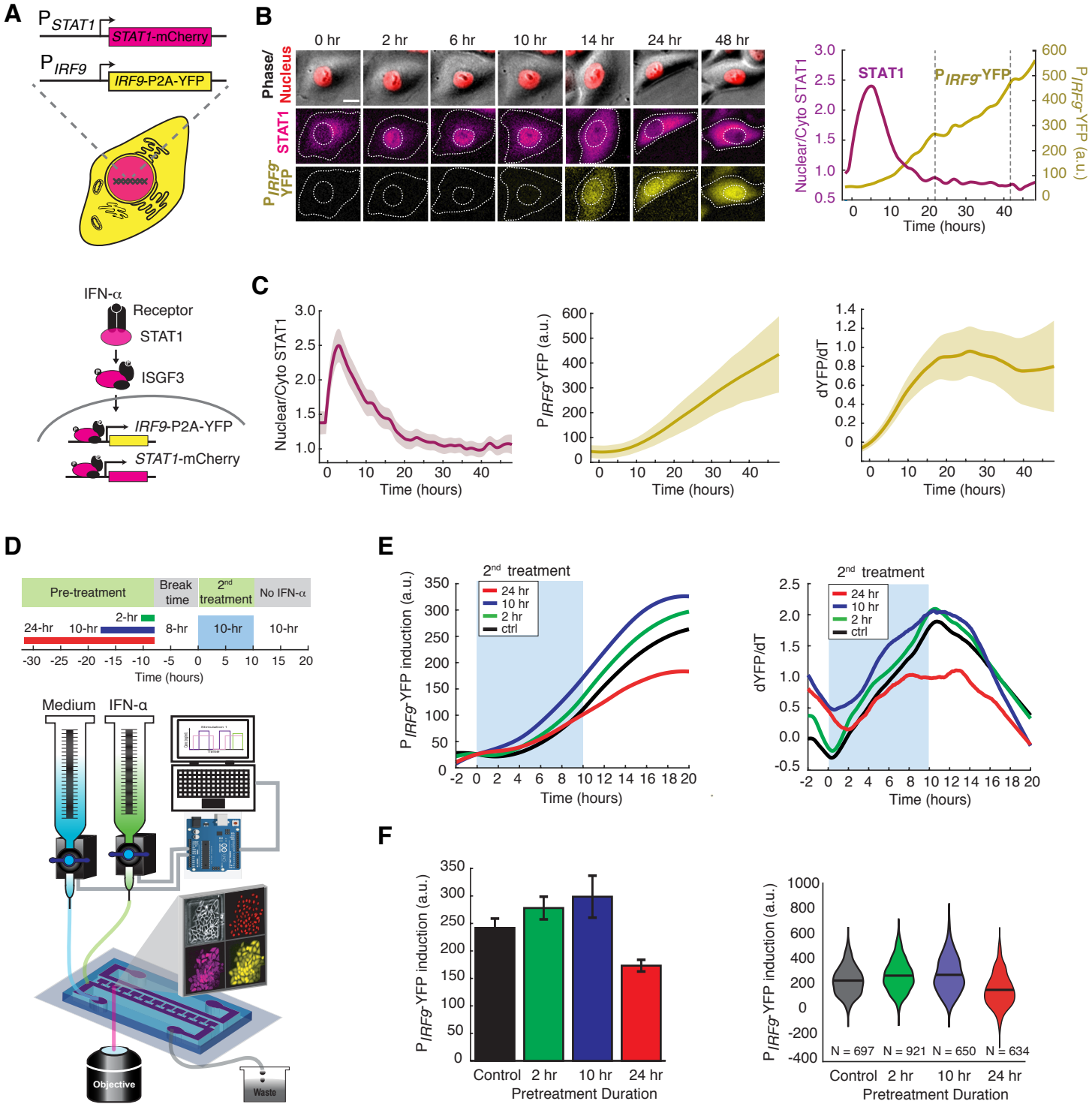
A
P STAT1
STAT1-mCherry
P IRF9
IRF9-P2A-YFP
IFN-α
Receptor
STAT1
ISGF3
IRF9-P2A-YFP
STAT1-mCherry
B
0 hr
2 hr
6 hr
10 hr
14 hr
24 hr
48 hr
Phase/ Nucleus
STAT1
P IRF9 YFP
Nuclear/Cyto STAT1
P IRF9 YFP (a.u.)
Time (hours)
C
Nuclear/Cyto STAT1
P IRF9 YFP (a.u.)
dYFP/dT
Time (hours)
D
Pre-treatment
Break time
2nd treatment
No IFN-α
24-hr
10-hr
2-hr
8-hr
Time (hours)
Medium
IFN-α
Objective
Waste
E
2nd treatment
24 hr
10 hr
2 hr
ctrl
P IRF9 YFP induction (a.u.)
dYFP/dT
Time (hours)
F
P IRF9 YFP induction (a.u.)
Control
2 hr
10 hr
24 hr
Pretreatment Duration
N = 697
N = 921
N = 650
N = 634

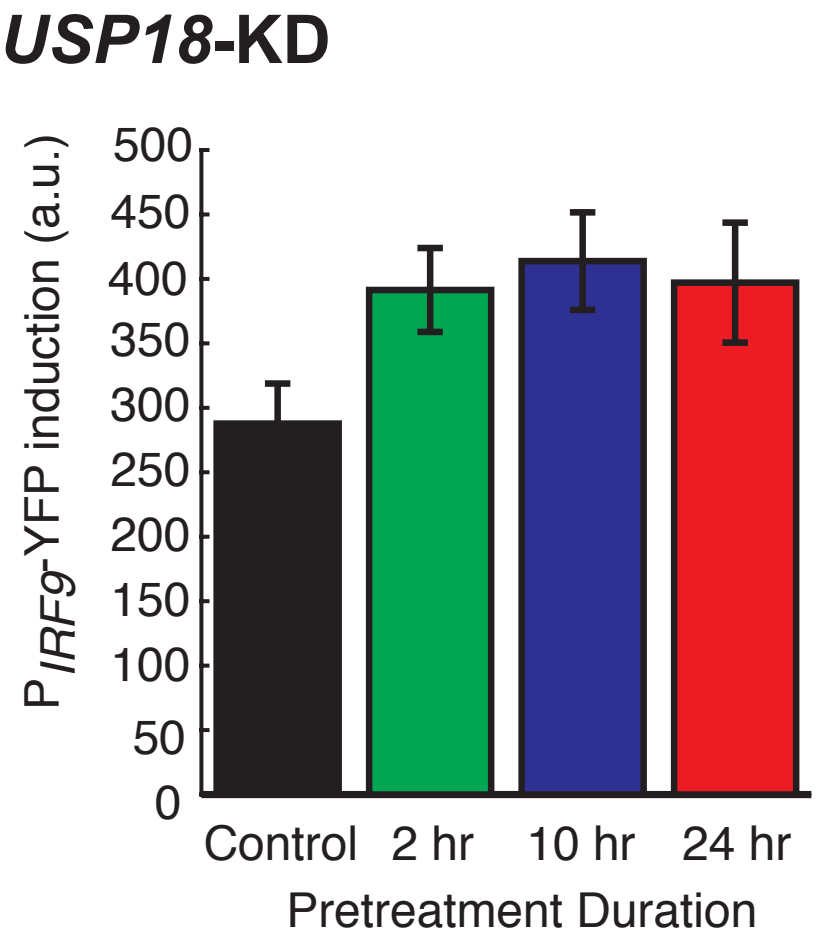

Figure2: Effect of USP18KO on IRF9 induction

Left: the bar graph of the average PIRF9 induction upon second IFN-alpha treatment in USP18-KD cells. Data are represented as mean ± SEM from 3 independent experiments. Right: the violin plot of PIRF9 induction upon second stimulation in single cells. The PIRF9 induction was calculated as the additional increase in YFP signal only to the second IFN-alpha treatment. The cells were combined from the 3 experiments.

Figure 3: Computational modeling suggests a delayed negative feedback loop

(A) A conceptual model of IFN-alpha induced differential expression kinetics of IRF9 and USP18. The delay time τ represents a continuous IFN stimulation lasted longer than a required threshold to activate USP18.

(B) The fitting error between simulations and the experiments performed by variation of the delay time while keeping all the other parameters free.

(C) The comparison between experimental data and the simulation for PIRF9 induction. The increase in PIRF9 expression to the second IFN-alpha treatment (data from figure 1F) was normalized to the no-pretreatment condition (control).

(D) The schematic of multiple pulses versus sustained experiment. Cells were treated with 100 ng/ml IFN-alpha for 8 hours, washed with PBS 3 times and left in the culture medium for 8 hours (break time). The procedure was repeated 5 times. In the sustained treatment condition, cells were treated with IFN-alpha for 40 hours and washed with PBS 3 times. After the last break time, images of the cells were captured, and fluorescent signals were quantified.

(E) The simulation of PIRF9-YFP induction in cells with USP18 (WT) and without USP18 (USP18KO). The level in each cell type was normalized to the multiple-pulse treatment.

(F) The experimental data of the average PIRF9-YFP induction in WT and USP18-KD cells. In each cell type, the induction level was first subtracted by the level in the untreated cells, then normalized to the 8-hr pulses condition. The error bars represent $\pm$ SD of the single cells.

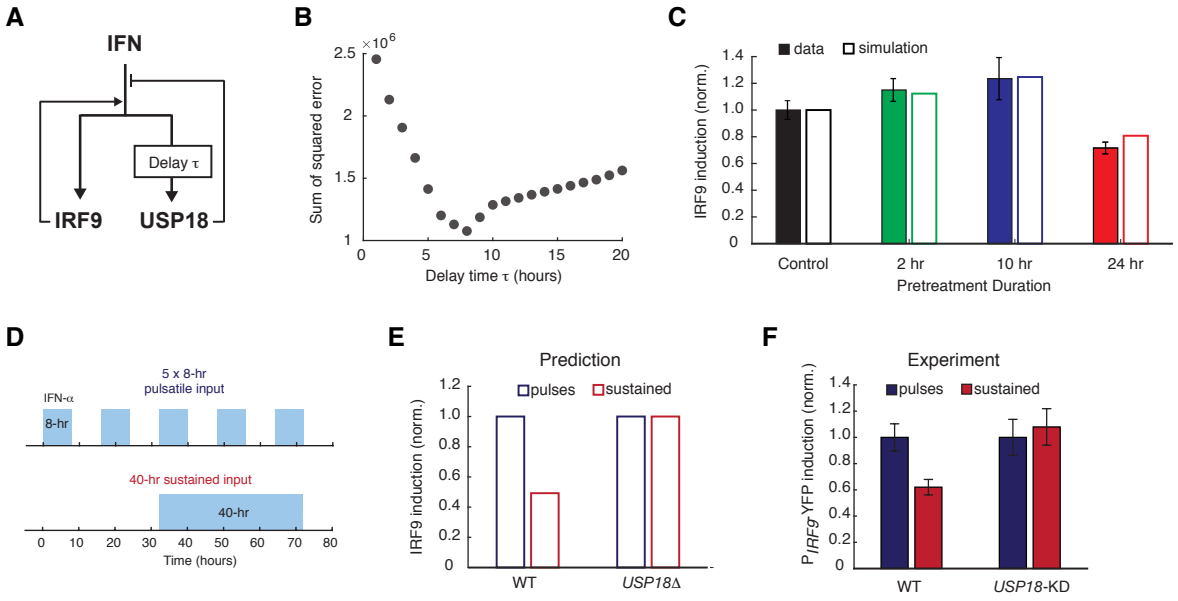
A
IFN
Delay τ
IRF9
USP18
B
×10^6
Sum of squared error
Delay time τ (hours)
C
data
simulation
IRF9 induction (norm.)
Control
2 hr
10 hr
24 hr
Pretreatment Duration
D
5 x 8-hr
pulsatile input
IFN-α
8-hr
40-hr sustained input
40-hr
Time (hours)
E
Prediction
pulses
sustained
IRF9 induction (norm.)
WT
USP18Δ
F
Experiment
pulses
sustained
P IRF9 YFP induction (norm.)
WT
USP18-KD

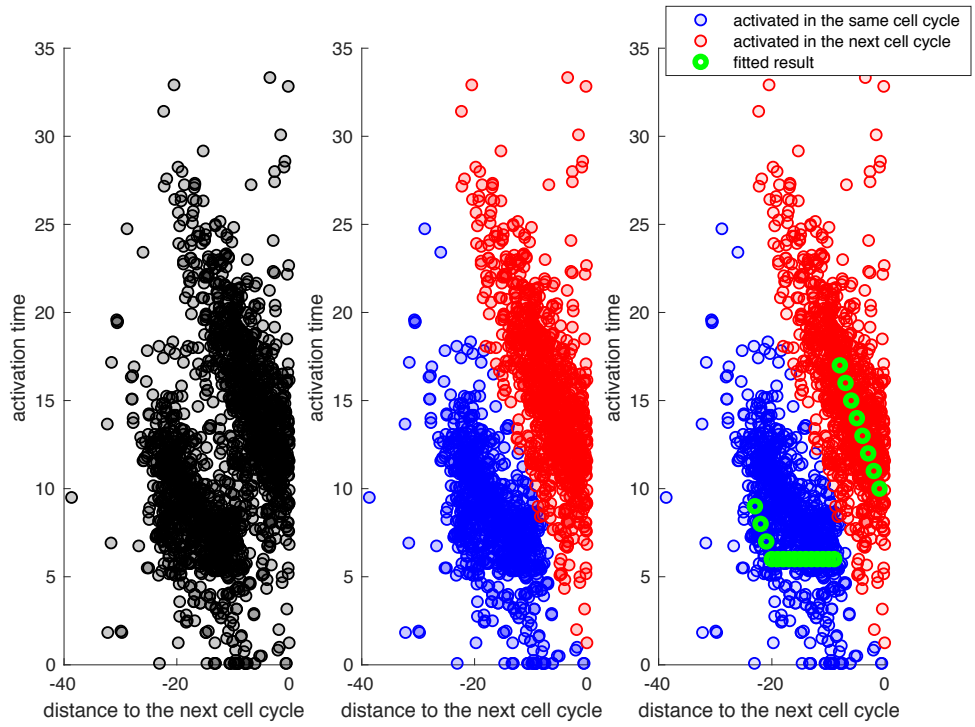

Figure4: USP18 activation is cell cycle dependent

Left panel: activation time of USP18 plotted against the relative time of now compared to the next cell cycle. First the time from stimulation to the next cell cycle is computed, denoted as t2. Then USP18 activation is plotted against -t2, where -t2 represents the relative time, in hour, from the onset of the stimulation to the next cell cycle.

Mid panel: if a cell activated USP18 before the cell divides, the cell will be colored blue. Otherwise it will be colored red. Evidently, the cells are well separated into two groups on the cell cycle trajectory.

Right panel: the fitted result based on adopting the window hypothesis is plotted on top of the original data.

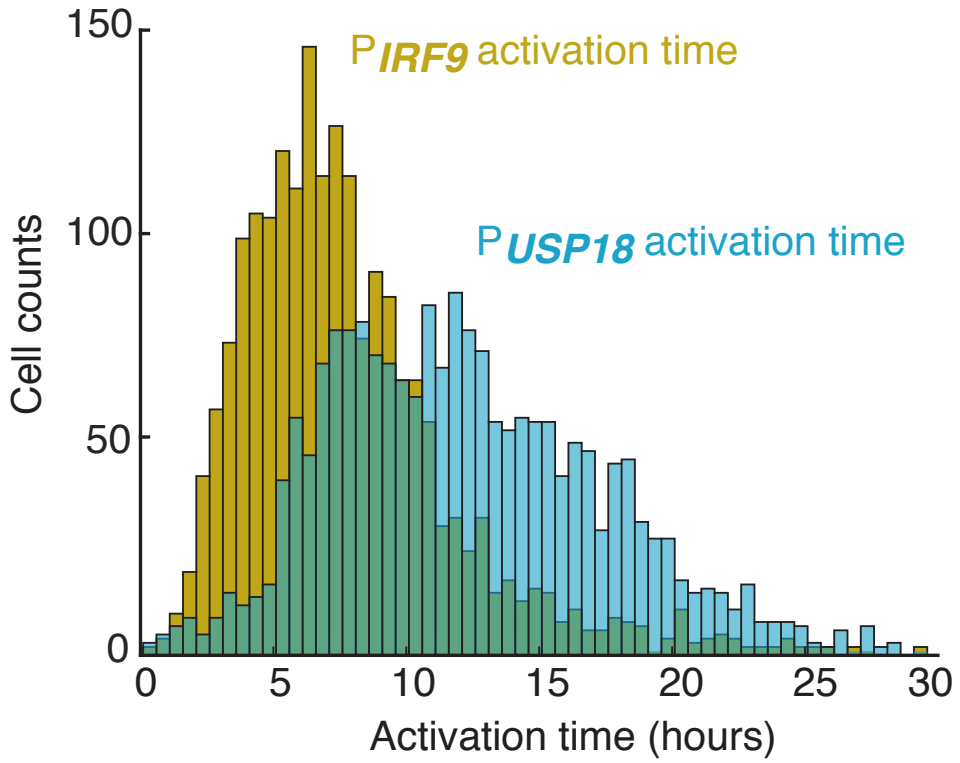

Figure5: activation time of USP18 and IRF9

The histograms of the activation time of USP18 and IRF9 are plotted on top of each other. The mean of IRF9 activation time is lower than that of USP18. More importantly, the spread of USP18 activation time is much larger than the spread of IRF9. Note that though the shape of IRF9 histogram looks symmetrical, that for USP18 look very biased toward long activation times.

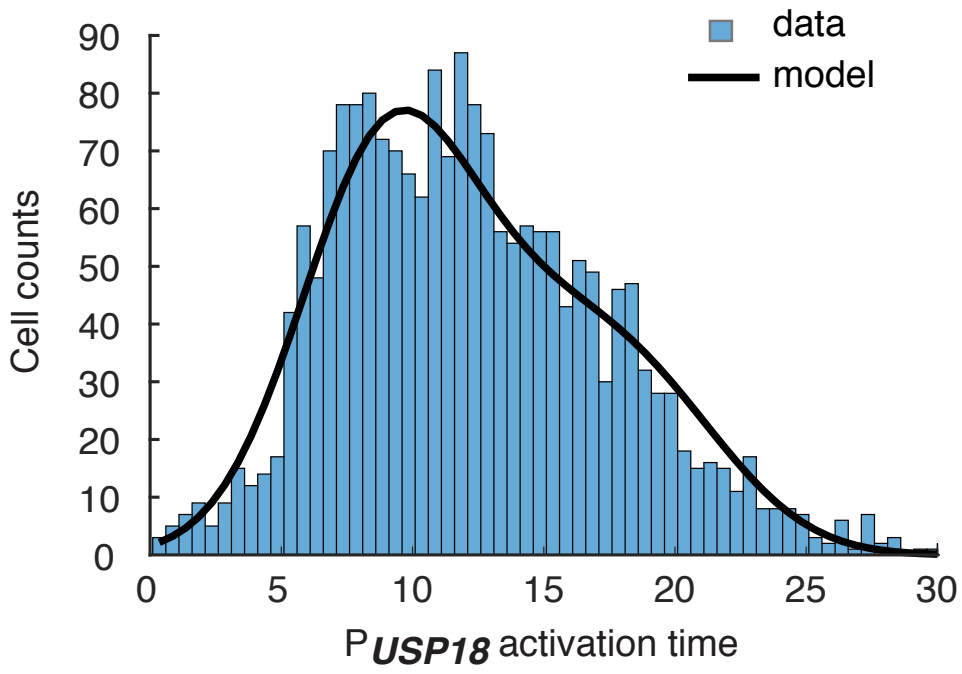

Figure 6: Fitted USP18 activation time histogram and USP18 activation time data

We assumed that the activation time observed can be broken down into a cell cycle independent and cell cycle dependent component, and the observed activation time is the sum of the two components. From our previous assumption, we can compute the distribution of the cell cycle dependent component. Since cell cycle independent component represents the time lost in signal transduction, DNA transcription, mRNA translation, and all kinds of chemical modifications on CFP, it is assumed to be gaussian, who's mean and variance will be obtained from data. By fitting the convolution of the distribution of the 2 components to the data, we inferred a biologically reasonable for cell cycle length and a window width that is consistent with previous findings.

References

1. Abreu, Sergio L., F. Carter Bancroft, and W. E. Stewart. "Interferon priming. Effects on interferon messenger RNA." Journal of Biological Chemistry 254.10 (1979): 4114-4118.

2. Stewart, William E., Lynn B. Gosser, and Royce Z. Lockart. "Priming: a nonantiviral function of interferon." Journal of Virology 7.6 (1971): 792-801.

3. Kuri, T., Zhang, X., Habjan, M., Martinez-Sobrido, L., Garcia-Sastre, A., Yuan, Z., Weber, F. "Interferon priming enables cells to partially overturn the SARS coronavirus-induced block in innate immune activation." Journal of General Virology 90.11 (2009): 2686-2694.

4. Isaacs, A., and D. C. Burke. 1958. Mode of action of interferon. Nature (London) 182:1073-1074.

5. Cheon, H., Holvey-Bates, E., Schoggins, J., Forster, S., Hertzog, P., Imanaka, N., Rice, C., Jackson, M., Junk, D., Stark,G. "IFNβ-dependent increases in STAT1, STAT2, and IRF9 mediate resistance to viruses and DNA damage." The EMBO journal 32.20 (2013): 2751-2763.

6. François-Newton, V., Almeida, G., Payelle-Brogard, B., Monneron, D., Pichard-Garcia, L., Piehler, J., Pellegrini, S., Uze, G. "USP18-based negative feedback control is induced by type I and type III interferons and specifically inactivates interferon α response." PLoS One6.7 (2011): e22200.

7. Sarasin-Filipowicz, M., Wang, X., Yan, M., Duong, F., Poli, V., Hilton, D., Zhang, D., Heim, M. "Alpha interferon induces long-lasting refractoriness of JAK-STAT signaling in the mouse liver through induction of USP18/UBP43." Molecular and cellular biology 29.17 (2009): 4841-4851.

8. Hersen, P., McClean,M., Mahadevan, L., Ramanathan, S. *Signal processing by the HOG MAP kinase pathway.* Proc Natl Acad Sci U S A, 2008. **105**(20): p. 7165-70.

9. Parker, Z., Pasieka,T., Parker, G., Leib, D. "Immune-and nonimmune-compartment-specific interferon responses are critical determinants of herpes simplex virus-induced generalized infections and acute liver failure." Journal of virology 90.23 (2016): 10789-10799.

10. Teijaro, J., Walsh, K., Rice, S., Rosen, H., Oldstone, M. "Mapping the innate signaling cascade essential for cytokine storm during influenza virus infection." Proceedings of the National Academy of Sciences 111.10 (2014): 3799-3804.

11. Purvis, J.E. and G. Lahav, Encoding and decoding cellular information through signaling dynamics. Cell, 2013. 152(5): p. 945-56.

12. Behar, M. and A. Hoffmann, Understanding the temporal codes of intra-cellular signals. Curr Opin Genet Dev, 2010. 20(6): p. 684-93.

13. Behar, M., Barken, D., Werner, S., Hoffmann, A. The dynamics of signaling as a pharmacological target. Cell, 2013. 155(2): p. 448-61.

14. Mitchell, A., P. Wei, and W.A. Lim, Oscillatory stress stimulation uncovers an Achilles' heel of the yeast MAPK signaling network. Science, 2015. 350(6266): p. 1379-83.

15. Mettetal, J.T., Muzzey, D., Gomez-Uribe, C., Oudenaarden, A. The frequency dependence of osmo-adaptation in Saccharomyces cerevisiae. Science, 2008. 319(5862): p. 482-4.

16. Hao, N. and E.K. O'Shea, Signal-dependent dynamics of transcription factor translocation controls gene expression. Nat Struct Mol Biol, 2012. 19(1): p. 31-9.